

## Experimental determination of the real elements of the density matrix of $H(n=3)$ atoms produced in 20–100-keV collisions of $H^+$ on Kr

N. Seifert,<sup>\*</sup> N. D. Gibson,<sup>†</sup> and J. S. Risley

*Atomic Collision Laboratory, Department of Physics, North Carolina State University, Raleigh, North Carolina 27695-8202*

(Received 14 June 1995)

In continuation of our previous work, charge transfer processes occurring in protons on rare-gas-atom collisions have been investigated. Diagonal and real off-diagonal coherence elements of the density matrix for  $H(n=3)$  atoms produced in 20–100-keV electron-capture collisions with Kr atoms are experimentally determined by analyzing the Balmer- $\alpha$  light from the decay of H atoms from the ( $n=3$ ) state to the ( $n=2$ ) state. The intensity and polarization of the emitted light are measured as functions of an axially symmetric electric field in the collision region. These data are fitted to a numerical model of the H atom in an electric field in order to extract density-matrix elements. The results are compared to previous studies of  $H^+$  on He and Ar. The collisionally produced dipole moment of the  $H(n=3)$  atom decreases for increasing atomic number of the rare-gas target atoms, which indicates that the final phase of the collision process is not essential for the formation of the dipole moment. This physical picture is further supported by our alignment data. Absolute cross sections for charge transfer to the  $3s$ ,  $3p$ , and  $3d$  levels are presented as well.

PACS number(s): 34.70.+e

### I. INTRODUCTION

The investigation of electronic processes in atomic collisions is of fundamental importance to our understanding of collision dynamics, and is also of practical relevance for a variety of fields such as astrophysics or fusion technology. In the 1980s and early 1990s simple systems such as protons on He were thoroughly studied both experimentally and theoretically [1–3]. The experimental technique used to investigate electron-capture into the  $n=2$  and 3 levels of H atoms was Stark mixing of the corresponding near degenerate opposite parity states and analyzing the emitted light in terms of its intensity and polarization. The impact-parameter-integrated density matrix is extracted by fitting the observed intensities and polarizations as a function of the applied field strength to a theoretical model [2]. The  $n$ -shell density-matrix elements provide the maximum possible information on the excited state of the H atom produced by the charge-transfer collision. Using the real elements of the  $n$ -shell density-matrix elements one can determine the average axially symmetric charge distribution (or probability density) and the dipole moment of the  $n$  state of the H atoms. The imaginary terms determine the current distribution in the  $n$  shell. Previous work has shown that the real parts of the density matrix are more easily measured using axial electric fields, and transverse fields give more precise results for the imaginary terms [4].

In continuation of the previous work by Risley and co-workers [4], we concentrate on investigating the charge distribution in the  $H(n=3)$  atoms produced by charge-transfer processes in proton on rare-gas-atom collisions employing an

axial electric field to Stark mix the  $n=3$  states. Simple collision systems such as  $H^+$  on He have been studied experimentally and theoretically intensively in recent years as mentioned above. While the most sophisticated computations seem to reproduce the experimental data quite well [5], an understanding of the physics behind the formation of, for example, the dipole moment has not yet been achieved. This is partly due to the lack of transparency of the theoretical models used. Theoretical work by Burgdörfer and Dubé [6,7] shows that the postcollisional interaction due to the Stark mixing of the states of the hydrogen atom by the electrical field of the receding ion does not influence or even produce a dipole moment in the “newborn” hydrogen atom. This is because the postcollision interaction (PCI) operator and the Runge-Lenz vector commute [7]. To our knowledge, this has yet to be shown experimentally. However, it is important to note that this simplified treatment of the PCI breaks down for small internuclear distances between the target ion and the projectile. The concept of the linear Stark effect works only for homogeneous and not too high electric fields, i.e., for not too small internuclear distances. Additionally, considerable overlap of the wave functions of the target and projectile occurs and has to be taken into account in the case of small internuclear distances. Therefore in our contribution PCI refers to electrostatic interaction of the captured electrons with the target ions (He, Ar, or Kr) at distances considerably larger than typical sizes of the atoms involved in the charge-transfer process.

Hippler *et al.* [8] investigated H and  $H^+$  on He collisions and observed that for investigated impact energies the collisionally formed dipole moment is smaller or even slightly negative (i.e., electron leads the proton) in the former case. The latter situation produces larger and positive dipole moments for impact energies greater than about 20 keV. Hippler *et al.* interpreted their data as evidence that the charge state of the target gas is of great importance for the formation of the dipole moment and the charge distribution in general. It

<sup>\*</sup>Present address: Institut für Allgemeine Physik, Technische Universität Wien, Wiednerhaupstr. 8-10, 1040 Wien, Austria.

<sup>†</sup>Present address: Physics Department, University of Wisconsin, 1150 University Avenue, Madison, WI 53706.

is important to realize that for H on He collisions the excited hydrogen atom is not affected by a receding ion but by an atom. One should also be aware of the fact that in the former case excitation has not been achieved by a charge-transfer process, but by direct excitation of the H atom. It is therefore difficult and problematic to compare both experimental situations.

A completely different interpretation of the formation of a dipole moment in ion-atom or atom-atom collisions is given by Aynacioglu, Neumann, and von Oppen [9] and Hanselmann, Aynacioglu, and von Oppen [10]. They believe that at least in collisions involving direct excitations inertial forces and not Coulomb forces are responsible for the formation of dipole moments in the He target atoms. They further interpret the fact that the observed dipole moments are quite large and that the  $m=0$  states are preferentially populated as an indication that the final phase of the collision process where the axis of the collision system is almost aligned with the ion beam is essential for the formation of the electric dipole moment. To our knowledge, their studies are the only ones which focus on the charge distribution of coherently excited nonhydrogenic states. However, the interpretation of the data in the case of nonhydrogenic systems is more difficult than in experiments where the density-matrix elements of hydrogen atoms are investigated. This is partly due to the fact that in the case of He one has to take into account electron correlation effects.

It is clear that although theoretical calculations have at least partly reproduced the experimental data for simple systems successfully, we do not know which physical properties of the constituents in an ion-atom collision are responsible for the occurrence of certain phenomena such as the formation of a dipole moment. From this perspective, using different target gases such as Kr, and using the very same technique which has proven its reliability and accuracy in previous experiments, bears the potential to provide valuable new information on the nature of processes which are ultimately responsible for charge transfer itself. Previous experiments [4] where the charge distribution for H( $n=3$ ) atoms produced in collisions with Ar atoms was studied showed a surprisingly small electric dipole moment (EDM) compared to the H<sup>+</sup> on He experiments. We extended our investigations to Kr target atoms in order to determine whether the observed phenomena are unique for H<sup>+</sup>-Ar collisions or are part of a general trend in proton-rare-gas-atom collisions. We present results of a study of formation of H( $n=3$ ) atoms by electron capture from a Kr target by 20–100-keV protons.

## II. APPARATUS

The experimental setup used in these experiments has previously been extensively described [1,2,4]. We used the same technique to investigate the optical properties (intensity and polarization) of the emitted light as the one used by Renwick *et al.* [4] who employed a photoelastic modulator (PEM) and photon-counting electronics. The light from the collision is observed similarly to previous studies through a standard manufacturer-specified bandpass of 10 nm centered at 656.2 nm. The Kr atoms has one weak Kr II line centered at about 657 nm that is visible through the filter. The ratio of Kr emitted light intensity to Balmer- $\alpha$  intensity was estimated

by comparing it to the intensity of light emitted in He<sup>+</sup>-Kr collisions, where the proton and He<sup>+</sup> projectiles had the same speed. It is known [11] that the emission cross sections are usually a factor of 2 to 3 higher for He<sup>+</sup>-rare-gas-atom collisions compared to H<sup>+</sup>-rare-gas-atom collisions at the same projectile speed. The amount of light emitted from the Kr target in He<sup>+</sup>-Kr collisions is therefore an upper limit for the unwanted background light emitted in H<sup>+</sup>-Kr collisions. The signal background turned out to be even smaller than the Ar background in the previous work of Renwick *et al.* [4] and has, therefore, only a negligible effect on our results. One can neglect this contribution because any intensity shift caused by the correction must be spread among the fitting functions (see next section), causing only small changes in their relative weights [4]. Thus the density-matrix elements, which are all normalized to the cross section for excitation of the  $n=3s$  level, suffer little change. We consequently neglected the weak Kr II line contribution.

## III. THE DENSITY MATRIX AND ITS INTERPRETATION

A hydrogen atom formed in a collision between a proton and a target gas atom at a particular impact parameter  $\mathbf{b}$  can be described by a pure state  $|\Psi(\mathbf{b})\rangle$ . This pure state may be expressed as a linear combination of the angular momentum eigenstates  $|nlm\rangle$  with amplitudes  $a_{nlm}(\mathbf{b})$ ,

$$|\Psi(\mathbf{b})\rangle = \sum_{n,l,m} a_{nlm}(\mathbf{b})|nlm\rangle. \quad (1)$$

In our experiment we observe only H( $n=3$ ) atoms by detecting emitted Balmer- $\alpha$  radiation. As a result, the summation in Eq. (1) is limited to  $n=3$  for this experiment. Furthermore, the H( $n=3$ ) atoms are observed regardless of impact parameter  $\mathbf{b}$  so that an ensemble of H( $n=3$ ) atoms is observed which is given by an incoherent superposition of states  $|\Psi(\mathbf{b})\rangle$  for all impact parameters  $\mathbf{b}$ . Because this ensemble is not in a pure state it is convenient to use a density matrix  $\sigma_3$  to describe the production of the H( $n=3$ ) atoms [12].

The elements of the density matrix  $\sigma_3$  follow from Eq. (1) as

$$\sigma_{lm'l'm'} = \int_0^{2\pi} \int_0^\infty a_{lm}(\mathbf{b}) a_{l'm'}^*(\mathbf{b}) b db d\phi, \quad (2)$$

where the amplitudes  $a_{lm}(\mathbf{b})$  refer to H( $n=3$ ) states. The density matrix  $\sigma_3$  has certain elements that are either identical to each other or zero because of symmetries in the collision. Because of these symmetries the  $9 \times 9$  H( $n=3$ ) density matrix  $\sigma_3$  has only 14 independent real parameters. This density matrix contains all of the information obtainable from our experiment about the production of H( $n=3$ ) atoms.

The complete information contained in the density matrix can be expressed in the associated electronic charge density distribution  $D(\mathbf{r})$  and current density distribution  $\mathbf{j}(\mathbf{r})$ . In this work only the charge density distribution was of interest. A first-order moment of  $D(\mathbf{r})$  is the average electric dipole moment  $\langle \mathbf{d} \rangle_z$  which for the H( $n=3$ ) density matrix is given by [13]

$$\langle \mathbf{d} \rangle_z = \frac{1}{\text{Tr}(\underline{\sigma}_3)} \text{Re}[6\sqrt{6}\sigma_{s_0p_0} + 6\sqrt{3}\sigma_{p_0d_0} + 18\sigma_{p_1d_1}]ea_0. \quad (3)$$

A positive value for  $\langle \mathbf{d} \rangle_z$  indicates that the electron lags behind the proton and a negative value indicates the electron leading the proton. The largest allowable value for  $\langle \mathbf{d} \rangle_z$  for  $H(n=3)$  is  $7.35ea_0$ .

#### IV. USE OF FITTING FUNCTIONS: DETERMINING THE DENSITY MATRIX

The procedure for analyzing the Stokes parameter data has been described in detail in previous publications [1,2,4], so we will give only a brief description here. The light observed is emitted from  $H(n=3)$  atoms formed all along the beam in the collision region and coherently excited into a linear superposition of substates with  $n=3$ , which will decay as they proceed down the beam line through the target cell. This superposition of states formed at the instant of capture is best described by a  $36 \times 36$  density matrix  $\underline{\sigma}_3$ . This matrix can be obtained by an analysis method that takes into account contributions to the Stokes parameters from all the different states and accounts for their time evolution as they proceed through the apparatus. Diagonal elements of  $\underline{\sigma}_3$  are the cross sections for capture to the various substates, while off-diagonal elements represent coherences of the capture process between the different eigenstates, averaged over all impact parameters and azimuthal angles.

This large matrix can be simplified by taking into account the axial and reflection symmetries. As a result of these symmetries, only 14 independent parameters are necessary to completely determine this matrix, whose elements are  $\sigma_{s_0}$ ,  $\sigma_{p_0}$ ,  $\sigma_{p_{\pm 1}}$ ,  $\sigma_{d_0}$ ,  $\sigma_{d_{\pm 1}}$ , and  $\sigma_{d_{\pm 2}}$ , and eight coherence elements,  $\text{Re}(\sigma_{s_0p_0})$ ,  $\text{Im}(\sigma_{s_0p_0})$ ,  $\text{Re}(\sigma_{s_0d_0})$ ,  $\text{Im}(\sigma_{s_0d_0})$ ,  $\text{Re}(\sigma_{p_0d_0})$ ,  $\text{Im}(\sigma_{p_0d_0})$ ,  $\text{Re}(\sigma_{p_{\pm 1}d_{\pm 1}})$ , and  $\text{Im}(\sigma_{p_{\pm 1}d_{\pm 1}})$ .

For a given density matrix, the intensity and polarization—the Stokes parameters—of the emitted light due to each of the matrix elements can be calculated from first principles. We use a numerical program to perform this calculation, which takes into account the time evolution of  $H$  atoms in our own particular experimental apparatus, including such effects as an accurate model of the electric field, the viewing region of the polarimeter, and the variation of the target number density as a function of distance along the  $z$  axis. Neglecting cascade, the measured Stokes parameters can be written as a sum of contributions from each of the density-matrix elements:

$$S_i(E) = \sum_{j,k} f_{ijk}(E)\sigma_{jk}, \quad (4)$$

where  $i$  is the Stokes parameter index and  $j$  and  $k$  are the angular momentum indices for the density matrix element  $\sigma_{jk}$ . The quantity  $f_{ijk}$  represents the optical contribution to Stokes parameter  $S_i$  from density-matrix element  $jk$  and is referred to as a “fitting function.” These fitting functions are calculated by the computer program. A linear statistical fit of the Stokes data to the fitting functions, in the form given by Eq. (5), yields the desired density-matrix elements.

Cascade from the  $n=4$  state is accounted for by use of another set of fitting functions  $g_{ijk}$ , calculated by a somewhat simplified procedure, where the hyperfine structure is neglected and solely elements of the  $H(n=4)$  density matrix with  $l \leq 1$  are used [2]. The two fitting function sets are combined for use in the fitting procedure.

In the previous work of Risley and co-workers [1,2], data were collected using both an axial and a transverse field. This required use of *two* sets of fitting functions,  $f_{ijk}^{(a)}$  for the axial field measurements and  $f_{ijk}^{(t)}$  for the transverse field. Both are required in order to measure precisely all the density-matrix elements. In this work, only an axial field was used, since only the charge distribution and not the current density distribution was of interest.

#### V. RESULTS

Table I shows the extracted density-matrix elements and dipole moments for 20-, 50-, 80-, and 100-keV proton impact energies. The error bars for most of the imaginary terms are very large. This is due to the fact that we only applied an axial electric field. However, the imaginary terms do not contribute to the charge density distribution, in which we are mainly interested. Reproducibility of the matrix elements and the dipole moment within quoted error bars is very good.  $\chi^2$ , which checks the goodness of the fit, varied between 0.5 and 0.9, indicating that the errors on the present results are properly determined.

Figure 1 shows that the dipole moments of the  $H(n=3)$  atoms for  $H^+$  on Kr are about 20–30 % lower than for  $H^+$  on Ar. Also the shapes are very similar in contrast to  $H^+$  on He.

The integral alignment  $A_{20}$  provides information about the relative population of the  $H(np_m)$  magnetic substates and is defined as [14,15]

$$A_{20}(n) = \frac{\sigma_{np_{\pm 1}} - \sigma_{np_0}}{2\sigma_{np_{\pm 1}} + \sigma_{np_0}}. \quad (5)$$

Please note that the  $\sigma_{np_{\pm 1}}$  denote the partial cross sections for excitation of either the  $m = +1$  or  $-1$  substate, which are identical due to the symmetry of the experimental setup [2].

A positive  $A_{20}$  indicates that the  $p_{\pm 1}$  states have been populated preferentially, whereas population of the  $m=0$   $p$  state corresponds to a negative alignment. In Fig. 2 the alignment is plotted for  $n=3$  in the case  $H^+$  on He and for  $n=3$  for  $H^+$  on Ar and Kr as a function of proton energy. One clearly sees the difference in alignment for He compared to either Ar or Kr targets in the investigated energy range. In the case of  $H^+$  on He the alignment  $A_{20}$  is negative for proton energies between 20 and 100 keV. For Ar or Kr targets the alignment is positive for impact energies between 20 and 40 keV, and is negative for large proton energies. Figure 2 shows the Ar and Kr alignment data are very similar.

The charge density (or probability) distributions of the electron in the  $H(n=3)$  atoms are plotted in Figs. 3 and 4. The  $H$  atoms move along the  $z$  axis from the left to the right. Density is indicated by height in Fig. 3 and by gray shading in Fig. 4. One can clearly see the displacement of the elec-

TABLE I. Density-matrix elements are shown for  $H(n=3)$  atoms produced in electron capture from Kr. The electric dipole moment is given in atomic units. All matrix elements have been normalized to the  $\sigma_{s_0}$  term.

Element	20 keV	50 keV	80 keV	100 keV
$s_0$	$1.00 \pm 0.17$	$1.000 \pm 0.063$	$1.000 \pm 0.061$	$1.000 \pm 0.099$
$p_0$	$0.341 \pm 0.105$	$0.165 \pm 0.043$	$0.192 \pm 0.044$	$0.118 \pm 0.073$
$p_1$	$0.585 \pm 0.064$	$0.139 \pm 0.019$	$0.110 \pm 0.017$	$0.101 \pm 0.027$
$d_0$	$-0.041 \pm 0.221$	$0.061 \pm 0.090$	$0.067 \pm 0.089$	$0.059 \pm 0.142$
$d_1$	$0.306 \pm 0.149$	$0.004 \pm 0.062$	$-0.013 \pm 0.063$	$0.003 \pm 0.102$
$d_2$	$0.013 \pm 0.039$	$0.024 \pm 0.017$	$0.029 \pm 0.016$	$0.021 \pm 0.027$
$\text{Re}(s_0 p_0)$	$-0.056 \pm 0.155$	$0.051 \pm 0.038$	$0.088 \pm 0.033$	$0.028 \pm 0.052$
$\text{Im}(s_0 p_0)$	$5.051 \pm 20.270$	$0.178 \pm 2.309$	$-2.557 \pm 1.419$	$0.603 \pm 1.803$
$\text{Re}(s_0 d_0)$	$-0.056 \pm 0.276$	$0.051 \pm 0.100$	$0.088 \pm 0.091$	$0.028 \pm 0.144$
$\text{Im}(s_0 d_0)$	$0.831 \pm 1.336$	$0.709 \pm 0.367$	$0.060 \pm 0.304$	$0.326 \pm 0.450$
$\text{Re}(p_0 d_0)$	$0.159 \pm 0.073$	$-0.012 \pm 0.015$	$-0.006 \pm 0.015$	$-0.019 \pm 0.025$
$\text{Im}(p_0 d_0)$	$-0.014 \pm 0.065$	$0.021 \pm 0.016$	$0.041 \pm 0.018$	$-0.020 \pm 0.029$
$\text{Re}(p_1 d_1)$	$0.246 \pm 0.092$	$0.069 \pm 0.021$	$0.031 \pm 0.018$	$0.054 \pm 0.029$
$\text{Im}(p_1 d_1)$	$-0.067 \pm 0.072$	$-0.010 \pm 0.022$	$0.049 \pm 0.021$	$-0.005 \pm 0.031$
$\chi^2$	0.65	0.77	0.9	0.53
$\langle dz \rangle$	$1.69 \pm 0.43$	$1.19 \pm 0.22$	$1.18 \pm 0.20$	$0.83 \pm 0.33$

tron to the trailing side of the atom. For energies near 20 keV the electron density is clearly high in the lobes on the side, which is due to the high population probability for the  $d_{\pm 1}$  states.

If the value of  $S_0(E=0)$  is *not* set equal to unity, the fitting procedure yields density-matrix elements (before normalization to  $\sigma_{s_0 s_0}$ ) in arbitrary but consistent units. Cross sections for capture to the  $3s$ ,  $3p$ , and  $3d$  levels can then be placed on an absolute scale by normalization at one energy to other groups' experimental results. This was previously done for the He target by Cline, Westerveld, and Risley [16], where relative He-target capture cross sections were normalized at 60 keV to the absolute results of Brower and Pipkin

[17]. The Kr results are placed on an absolute scale by using the Baratron capacitance manometer to calibrate the ion gauge [4]. The results are shown in Fig. 5. Similarly to the Ar and He cases the cross section for charge transfer into the  $3s$  orbitals maximizes somewhere close to 50 keV, whereas the cross sections for both the  $3p$  and  $3d$  orbitals decreases monotonically in the investigated proton energy regime. Our results are compared to the cross sections obtained by Lenormand [18]. Good agreement is seen for the  $3p$  and  $3d$  capture cross sections, whereas the agreement is poor for capture into the  $3s$  state.

## VI. DISCUSSION

The main aim of the  $H^+$  on rare-gas-atom collision experiments is to investigate and, if possible, to determine the physical factors which account for the observed collisionally produced charge density distributions of the  $H(n=3)$  atoms. It can be clearly seen from Fig. 1 that the EDM decreases for target gases with larger atomic numbers. Since in all cases the newly formed H atom is affected by an ion with charge  $q=+1$  for large separations, electrostatic forces acting upon the  $H(n=3)$  atoms in the final phase of the collision process, where the only influence due to the presence of the ion is its charge state, cannot account for the observed dependence of the EDM as a function of the target gas.

As already mentioned in the Introduction of this paper, Aynacioglu and co-workers [9,10] interpret their data in terms of inertial forces rather than Coulomb forces on the charge cloud during the collision process. They found that the magnitude of EDMs produced in target gas atoms by direct excitation is independent of the charge state of the incoming ions. Maraglia and Rodriguez [19] calculated that the collisionally produced hydrogen EDMs in  $A^{q+}$ -H collisions is fairly independent of the incident charge state for charge states  $q=1, 2$ , and 4, but the EDM reverses sign for charge state  $q=-1$ . Krotkov and Stone [20] and Hippler [3]

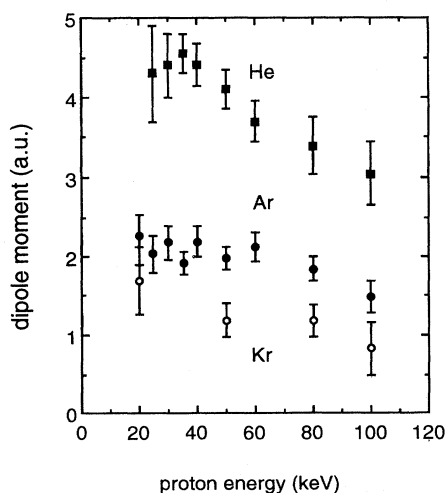


FIG. 1. The dipole moment for  $H(n=3)$  atoms produced by electron capture from He (■) (Refs. [2,4]), Ar (●) (Ref. [4]), and Kr (○) targets is plotted as a function of proton energy. The dipole moment decreases for increasing atomic number.

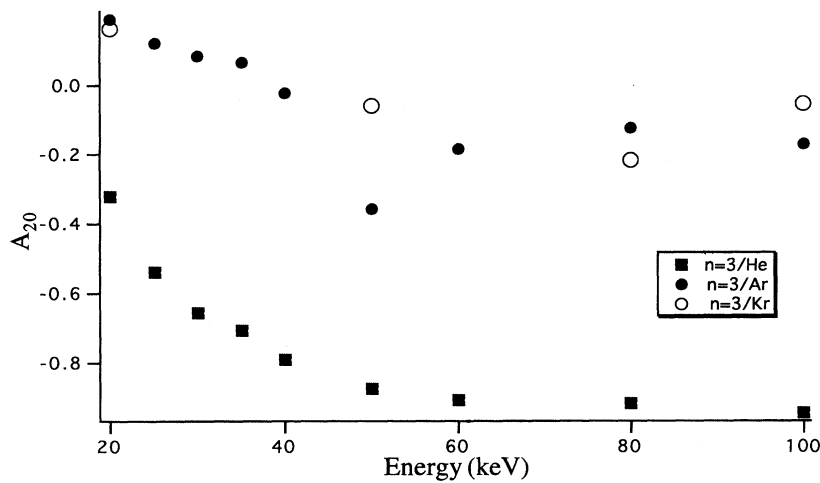
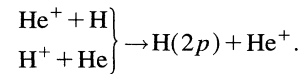


FIG. 2. The integral alignment  $A_{20}$  plotted against incident proton energies for  $H^+$  on  $He(n=3)$  (Refs. [2,4]),  $Ar(n=3)$  (Ref. [4]), and  $Kr(n=3)$  collisions. The integral alignment in the case of Kr and Ar is positive for small proton energies, which indicates preferential population of  $p_{\pm 1}$  states.

measured the EDM of  $H(n=2)$  states excited by H atom impact on He and found a negative EDM. A question arises at this point: what causes the variety of different and partly seemingly contradicting results? Recent experiments performed by Hippler *et al.* [21] seem to indicate that spin effects can be made responsible for the variety of observed results. The authors investigated the following reaction channels:



In a one-electron picture one would not expect that the alignment, for instance, differs for the different reaction channels at small velocities. In a one-electron picture the only difference is due to the fact that in the  $H^+$  on He case,  $H(2p)$

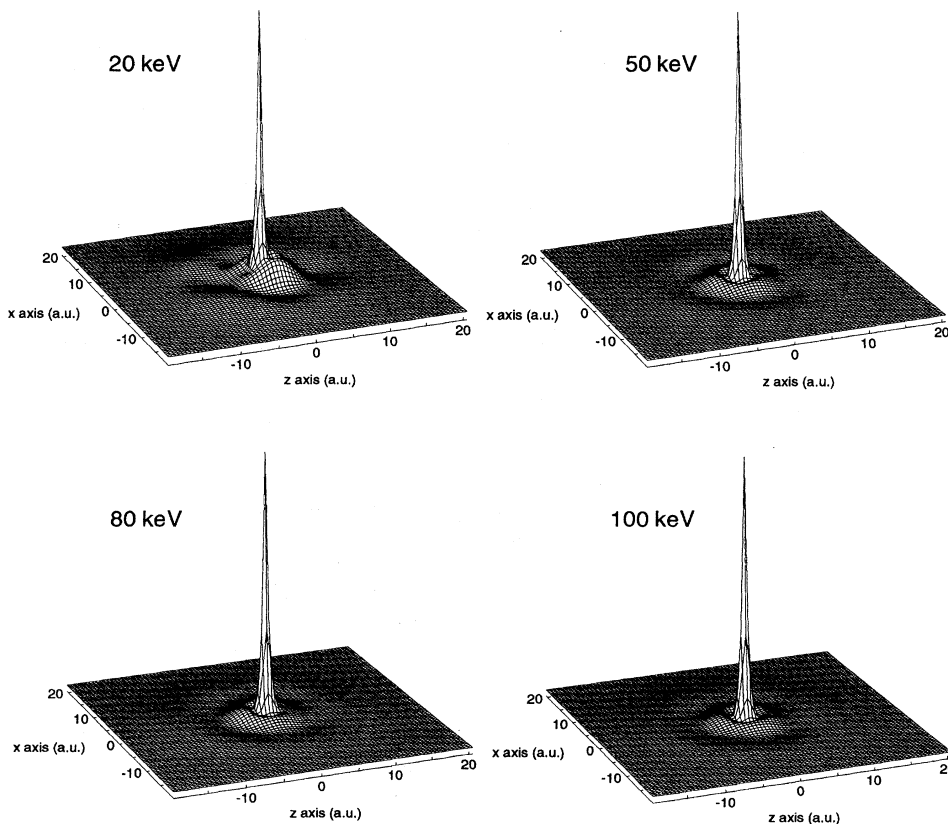


FIG. 3. Probability density in the  $x$ - $z$  plane for the H atom. Density is indicated by height, with the vertical axis on each plot normalized to the plot's highest density. The beam direction is along the  $z$  axis, with the atom moving to the right.

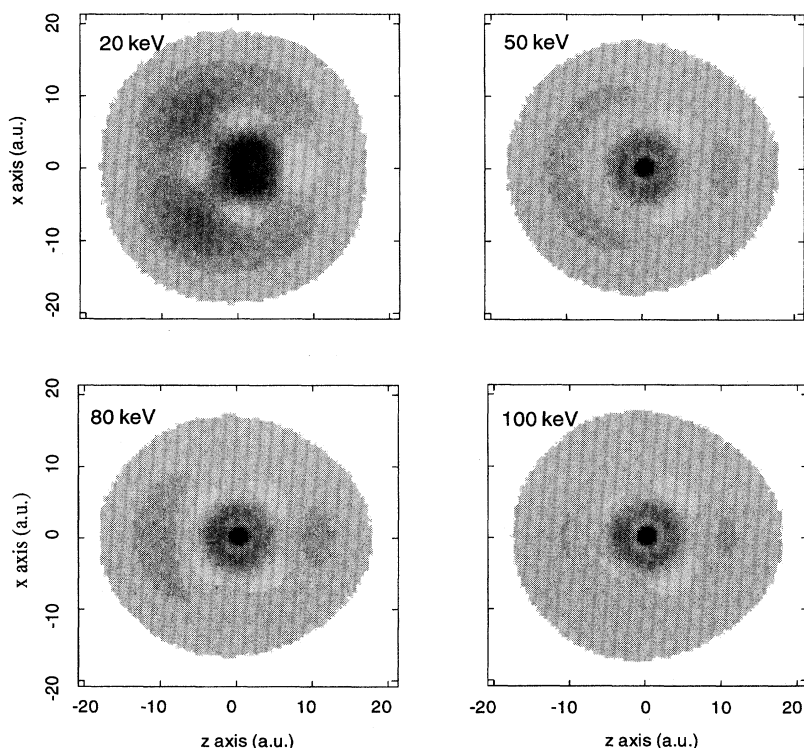


FIG. 4. Charge density distribution  $D(r)$  in the  $x$ - $z$  plane.  $D(r)$  is indicated by shading. The H atom is traveling to the right. The box indicates the range from  $-20a_0$  to  $20a_0$ . The high occupation probability of the  $d_{\pm 1}$  states is clearly indicated by the high occupation probability at the lobes in the case of 20 keV.

population arises from a two-step mechanism (radial  $1s\sigma$ - $2p\sigma$  coupling and rotational  $2p\sigma$ - $2p\pi$  or radial  $2p\sigma$ - $2s\sigma$  coupling), whereas only the latter coupling mechanisms ( $2p\sigma$ - $2p\pi$  or  $2p\sigma$ - $2s\sigma$ ) dominate in the second reaction channel for the production of  $H(2p)$ . Since both reaction channels appear to proceed along the same intermediate states and through the same couplings, one would therefore expect to observe the same alignment in both cases. However, in a two-electron picture, where electron correlation effects are considered, the situation changes and the reaction channels do not proceed via the same couplings. The relative population of  $2p_0$  and  $2p_{\pm 1}$  clearly depends on whether the process proceeds along the triplet or the singlet channel. This channel dependence has been shown theoretically and ex-

perimentally by Hippler *et al.* [28]. Spin effects could at least partly account for the large variety of results observed for different incident ions and target gases. Additionally, one would expect a difference in the final charge distribution depending on whether the collision dynamics proceeds via the charge transfer (as in our experiments)—or the direct excitation channel (Refs. [3,9,10,20]).

However, in the experiments reported here, spin effects do *not* influence the results. This is because there exists only one (singlet) channel. Our results are consequently clearly easier to interpret in terms of charge state influence or electron correlation effects of the target gas on the charge distributions of the collisionally produced  $H(3n)$  atoms. Based on the fact that the EDM of the  $H(n=3)$  depends on the atomic

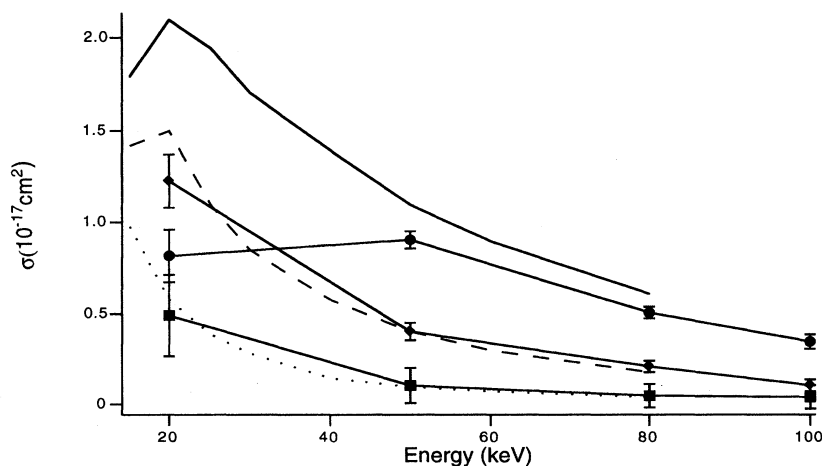


FIG. 5. Absolute capture cross sections for protons on Kr are displayed:  $\bullet$ , capture to the  $3s$  state, present results;  $\blacklozenge$ , capture to the  $3p$  state, present results;  $\blacksquare$ , capture to the  $3d$  state, present results; solid line, capture to the  $3s$  state, Ref. [18]; dashed line, capture to the  $3p$  level, Ref. [18]; dotted line, capture to the  $3d$  state, Ref. [18]. The error bars reflect random errors only. The normalization to the He cross section adds an overall error of 20%.

number of the rare-gas target atoms we believe that the processes which determine the magnitude of the EDM are dominant in the near collision region and are further related to the Coulomb force of the target ions and electron-electron interactions.

It is known that the cross sections for producing  $H(n=3)$  states increases with increasing atomic number [2,4,18]. This then implies a larger impact parameter range for Kr and Ar compared to He and the average impact parameter is consequently larger in the former case. A larger impact parameter corresponds to less drag on the captured electron by the singly ionized target atom. A smaller drag of the target ion induces a smaller elongation of the charge cloud of the newly formed  $H(n=3)$  atom and therefore leads to a smaller EDM, in accordance with our observations. The charge-transfer cross section, on the other hand, increases for smaller ionization energy, since the release condition is satisfied for a larger range of impact parameters as observed experimentally. The classical Bohr-Lindhard model (BLM) [22] gives surprisingly good results in the case of collisions of fully stripped ions with hydrogen and correctly predicts the cross sections for charge transfer in a very wide range of impact velocities [23]. It is important to note that the BLM accounts only for total cross sections and not for cross sections into subshells or charge distributions. This is not surprising, since the BLM is a “classical” model. However, one can use the BLM to roughly estimate the drag of the target ion on the hydrogen electron at the moment of capture, i.e., in the near collision region. Using the ionization energies of He, Ar, and Kr [24], one can calculate the ratio of the Coulomb forces of the target gas ions to be roughly 2.4 for He and Ar and 1.3 for Ar and Kr. The observed ratios of the EDMs are 2 for He and Ar, and 1.3 for Ar and Kr. Our rough estimate did not consider electron correlation effects, which should decrease the EDM further. However, the purpose of this rough estimate is to explain the observed tendency of our EDM data. The decrease of the EDMs is therefore consistent with Coulomb forces of the receding target ions, acting in the near collision region, and pulling the transferred electron back. The drag on the captured electron is not considered to be a PCI effect, since it occurs at internuclear distances where the concept of the linear Stark effect (i.e., homogeneous electric field) breaks down. It is further important to recall that the BLM is a model based on very simple and nonquantum-mechanical considerations. It is therefore possible that the observed decrease of the EDMs for increasing atomic numbers is a purely quantum-mechanical effect and is not correlated with electrostatic forces acting in the near collision region. The results of our very simple considerations are therefore valid qualitatively only (at best).

Preliminary results of more sophisticated computations performed by Lundy and Olson [25] confirm that the EDM decreases for Ar, and Kr with respect to He. At a proton impact energy of 50 keV the classical trajectory Monte Carlo computations (CTMC) predict that the ratio of the EDMs of He to Ar and Ar to Kr should be about 1.5 and 1.2, respectively.

The higher density of electrons in the case of Kr targets with respect to Ar and He could also result in a pushing of the transferred electron closer to the proton, which would decrease the EDM further.

Our results are consistent with investigations performed by Siegmann *et al.*, [26] who investigated the EDMs of  $H(n=2)$  atoms produced in  $H^+$ -Ar collisions at lower energies. For energies around 15 keV and higher, the collisionally produced EDMs are somewhat smaller than the EDMs produced in  $H^+$ -He collisions [3]. However, the error bars in the work of Siegmann *et al.* are too large to quantitatively compare their results to ours.

Another difference between the Kr (and Ar) and the He data is that the integrated alignment  $A_{20}$  is considerably larger and even positive for small impact energies in the former case (Fig. 2). This is consistent with results presented by Teubner *et al.* [27] and Hippler *et al.* [28] who investigated the integral alignment in  $H^+$ -rare-gas-atom collisions (He and Ar) for electron capture into the  $H(2p)$  states. In the case of Ar the population of the  $p_{\pm 1}$  states is larger than that of the  $p_0$  state (i.e., positive alignment) in contrast to He for proton energies around 20 keV, whereas the sign of the integral alignment changes for energies larger than about 30–40 keV in accordance with our  $n=3$  Ar and Kr data (see Fig. 2). Polarization data of the Lyman- $\alpha$  line emitted in  $H^+$ -Kr collisions indicate that the integral alignments of Ar and Kr are also very similar in the  $n=2$  case [31,29]. Even for energies as large as 100 keV the population probability of the  $p_{\pm 1}$  states is only slightly smaller than that of the  $p_0$  state in contrast to  $H^+$ -He collisions (Table I and Fig. 2). The fact that the integral alignment is similar for  $n=2$  and 3 excitation indicates that  $2p\sigma$ - $3p\sigma$  (separated atom notation) radial couplings are dominant in all cases (He, Kr, and Ar) [30] for proton energies between 20 and 100 keV. The reason for the large population of the  $p_{\pm 1}$  states is presently unknown. One possible explanation might be that in contrast to He, the ground states of Ar and Kr have  $s$ - and  $p_{0,\pm 1}$ -state contributions which couple presumably to different states with different strengths. The fact that the hydrogen  $m=0$  states are *not* preferentially excited in the case of  $H^+$  on Ar or Kr in contrast to  $H^+$  on He [1,2,4] provides further evidence that no forces of any kind acting in the final phase of the collision, where the internuclear axis is parallel to the  $z$  axis, can account for the observed alignment or EDM. Formation of the EDMs of hydrogen atoms seems to occur during the close encounter.

The population probability of the  $d_{\pm 1}$  states is very similar to that of the  $p_{\pm 1}$  states in the case of Kr and Ar [4]. For small impact energies the occupation of  $d_{\pm 1}$  dominates the  $d_0$  and  $d_{\pm 2}$  occupation. This changes clearly for impact energies higher than about 50 keV. This similarity could serve as an indication of the importance of  $2p\sigma$ - $3d\sigma$  and  $2p\pi$ - $3d\pi$  radial couplings at low impact energies. It is striking that the  $m=\pm 1d$  states are mainly populated at low proton energies and not the  $m=\pm 2d$  states which would geometrically correspond to the  $m=\pm 1p$  states. Therefore a pure geometrical interpretation, where the electron is pulled back by the target ion, cannot provide a complete explanation of the observed charge distribution data. Quantum-mechanical effects, such as radial couplings etc., need to be taken into account as well.

The probability density for the wave function describing the H atom shortly after the electron capture can be calculated from the density-matrix elements. Similar to the Ar experiments, as discussed above, one can see that the elec-

tron cloud not only lags behind the proton but also wraps around it to the sides, giving the cloud a horseshoe shape (see Figs. 3 and 4) for small impact energies. Probability (or charge) density plots offer a beautiful and very comprehensive way to graphically present the collisionally induced charge distribution.

The absolute cross sections for charge transfer to the  $3s$ ,  $3p$ , and  $3d$  H atom states for  $H^+$  on Kr are compared to the corresponding data of Lenormand [18]. The agreement in the case of the  $3s$  capture cross section is poor. However, Lenormand's cross sections are also in variance with our recently obtained  $3s$  capture cross sections in the case of Ar, which are in good agreement with data measured by Hughes *et al.* [31]. Similarly to the Ar and He cases, the capture cross section for capture into the  $3s$  state maximizes at energies somewhere between 20 and 50 keV, whereas the capture cross section for capture into the  $3p$  and  $3d$  levels decreases in the investigated energy region. This is in good agreement with the data obtained by Lenormand.

## VII. CONCLUSIONS

Real elements of the density-matrix elements of  $H(n=3)$  atoms produced in  $H^+$  on Kr atom collisions were determined experimentally in this work. The charge density distribution, whose computation is based on the measured density-matrix elements, indicates that electrostatic postcollisional interaction does not influence the formation of an electric dipole moment in the  $H(n=3)$  atoms. The observed integral alignment of the  $3p$  states is consistent with previous results where the  $n=2$  alignment was investigated. For proton energies around 20 keV the  $m=1$  ( $p$  and  $d$ ) states are preferentially occupied, similarly to results of recently performed  $H^+$  on Ar experiments, and in contrast to  $H^+$  on He experiments.

## ACKNOWLEDGMENTS

The fitting functions were calculated at the Cornell National Supercomputing Facility, whose support is acknowledged. This work was supported by the National Science Foundation under Grant No. PHY90-16986.

- 
- [1] C. C. Havener, N. Rouze, W. B. Westerveld, and J. S. Risley, *Phys. Rev. A* **33**, 276 (1986).
  - [2] J. R. Ashburn, R. A. Cline, P. J. M. van der Burgt, W. B. Westerveld, and J. S. Risley, *Phys. Rev. A* **41**, 2407 (1990).
  - [3] R. Hippler, *J. Phys. B* **26**, 1 (1993).
  - [4] S. P. Renwick, E. C. Martell, W. D. Weaver, and J. S. Risley, *Phys. Rev. A* **48**, 2910 (1993).
  - [5] M. Kimura, *Phys. Rev. A* **44**, R5339 (1991).
  - [6] J. Burgdörfer and L. J. Dubé, *Phys. Rev. Lett.* **52**, 2225 (1984).
  - [7] J. Burgdörfer and L. J. Dubé, *Nucl. Instrum. Methods Phys. Res. Sect. B* **10/11**, 198 (1985).
  - [8] R. Hippler, O. Plotzke, W. Harbich, H. Madeheim, H. Kleinpoppen, and H. O. Lutz, *Phys. Rev. A* **43**, 2587 (1991).
  - [9] A. S. Aynacioglu, S. Heumann, and G. von Oppen, *Phys. Rev. Lett.* **64**, 1879 (1990).
  - [10] M. Hanselmann, A. S. Aynacioglu, and G. von Oppen, *Phys. Lett. A* **175**, 314 (1993).
  - [11] E. W. Thomas, *Excitation in Heavy Particle Collisions* (Wiley, New York, 1972).
  - [12] K. Blum, *Density Matrix Theory and Applications* (Plenum, New York, 1981).
  - [13] C. C. Havener, W. B. Westerveld, J. S. Risley, N. H. Tolk, and J. C. Tully, *Phys. Rev. Lett.* **48**, 926 (1982).
  - [14] U. Fano and J. H. Macek, *Rev. Mod. Phys.* **45**, 553 (1973).
  - [15] K. Blum and H. Kleinpoppen, *Phys. Rep.* **52**, 203 (1979).
  - [16] R. A. Cline, W. B. Westerveld, and J. S. Riley, *Phys. Rev. A* **43**, 1611 (1991).
  - [17] M. C. Brower and F. M. Pipkin, *Phys. Rev. A* **39**, 3323 (1989).
  - [18] I. Lenormand, *J. Phys. (Paris)* **37**, 699 (1976).
  - [19] J. E. Maraglia and V. D. Rodriguez, in *Proceedings of the 17th International Conference on Physics of Electronic and Atomic Collisions*, edited by W. R. MacGillivray, I. E. McCarthy, and M. C. Standage (Hilger, Bristol, 1992).
  - [20] R. Krotkov and J. Stone, *Phys. Rev. A* **22**, 473 (1980).
  - [21] R. Hippler, H. Madeheim, H. O. Lutz, M. Kimura, and N. F. Lane, *Phys. Rev. A* **40**, 3446 (1989).
  - [22] N. Bohr and J. Lindhard, *K. Dan. Vidensk. Selsk. Mat. Fys. Medd.* **28**, No. 7 (1954).
  - [23] H. Knudsen, H. K. Haugen, and P. Hvelplund, *Phys. Rev. A* **23**, 597 (1981).
  - [24] B. H. Bransden and C. J. Joachain, *Physics of Atoms and Molecules* (Longman, New York, 1983), p. 302.
  - [25] C. J. Lundy and R. E. Olson (private communication).
  - [26] B. Siegmann, G. Tepehan, R. Hippler, H. Madeheim, H. Kleinpoppen, and H. O. Lutz, in *Proceedings of the 18th International Conference on the Physics of Electronic and Atomic Collisions*, edited by T. Andersen, B. Fastrup, H. Falkmann, and H. Knudsen, Abstracts of contributed papers Vol. II (Aarhus University Press, Aarhus, 1993), p. 553.
  - [27] P. J. O. Teubner, W. E. Kauppila, W. L. Fite, and R. J. Girmius, *Phys. Rev. A* **2**, 1763 (1970).
  - [28] R. Hippler, W. Harbich, M. Faust, H. O. Lutz, and L. J. Dubé, *J. Phys. B* **19**, 1507 (1986).
  - [29] B. Van Zyl, M. W. Gealy, and H. Neumann, *Phys. Rev. A* **35**, 4551 (1987).
  - [30] M. Kimura, *Phys. Rev. A* **44**, R5339 (1991).
  - [31] R. H. Hughes, C. A. Stigers, B. M. Doughty, and E. D. Stokes, *Phys. Rev. A* **1**, 1424 (1970).

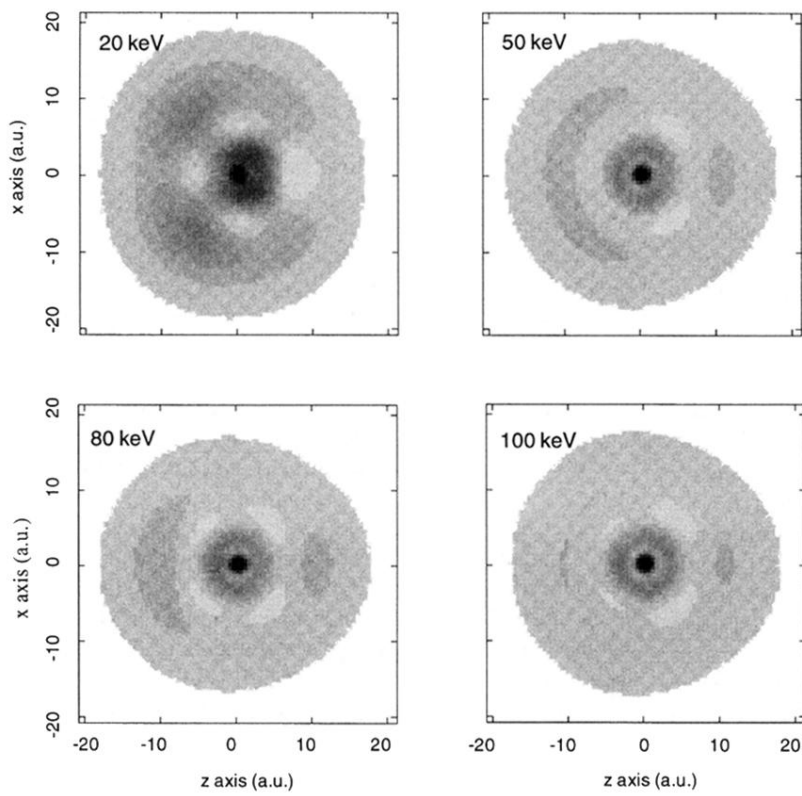


FIG. 4. Charge density distribution  $D(r)$  in the  $x$ - $z$  plane.  $D(r)$  is indicated by shading. The H atom is traveling to the right. The box indicates the range from  $-20a_0$  to  $20a_0$ . The high occupation probability of the  $d_{\pm 1}$  states is clearly indicated by the high occupation probability at the lobes in the case of 20 keV.